UAV-Based Antenna Measurements for Polarimetric Weather Radars: Probe Analysis

ARTURO Y. UMEYAMA, (Member, IEEE),
JORGE L. SALAZAR-CERRENO, (Senior Member, IEEE),
AND CALEB FULTON, (Senior Member, IEEE)

Advanced Radar Research Center, The University of Oklahoma, Norman, OK 73019, USA
School of Electrical and Computer Engineering, The University of Oklahoma, Norman, OK 73019, USA

Corresponding author: Jorge L. Salazar-Cerreno (salazar@ou.edu)

ABSTRACT One of the principal challenges in the calibration of polarimetric weather radars is achieving the strict requirements in the measurement of the antenna radiation pattern of the system; e.g., a co-polarization mismatch of at most 0.1 dB, and cross-polarization levels less than approximately −40 dB are highly desirable. In a UAV-based antenna pattern measurement system, the radiation characteristics of the probe antenna can be adversely affected by scattering off of the UAV platform itself, and by the relative orientation of the probe antenna with respect to the UAV frame. It is hypothesized that such extraneous reflections depend on the type of antenna used as a probe, and in this context, a more directive probe antenna (i.e., with low back lobe radiation) would be necessary to achieve the required measurement accuracy for weather radar applications. This work studies the effect of UAV and probe antenna interaction for different types of antennas through EM simulations, and this is validated with chamber measurements. For the patch array antenna under study, co-polarization mismatch levels of approximately 0.13 and 0.05 dB, and maximum cross-polarization levels of −37 and −34 dB, are achieved at boresight in measurements and simulations, respectively, which can be improved to meet the requirements with a careful selection of the gimbal operating angle range.

INDEX TERMS Antenna characterization, co-polarization mismatch, cross-polarization contamination, dual-polarized, far-field, measurements, probe, UAV interaction, weather radar.

I. INTRODUCTION

With the introduction of dual-polarized multifunction phased array weather radar systems (MPAR) [1] as a replacement for the current dish-based weather radar system (WSR-88D), additional challenges arise in the characterization and calibration of their components to ensure that no biases are being introduced in the polarimetric weather radar products [1], [2]. Namely, strict requirements on the mismatch between the co-polarization patterns of no greater than 0.1 dB, and cross-polarization levels of no greater than about -40 dB, are imposed, since the radiation properties in phased array antennas depend on the electronic scanning direction [3]. Typically, an outdoor in-situ range can be built to ade-

quately measure the antenna system's performance in its final installation site to ensure that it meets the requirements, and that its interaction with the environment is predictable [4], [5]. Unfortunately, it can easily become cost-prohibitive and impractical to develop outdoor RF antenna ranges for networks with a large number of immovable radars. Thus, an in-situ antenna measurement method that complies with such demands is ideal for characterization and calibration.

The field of RF measurement and characterization using UAVs, ranging from micro and small to medium and large frames, has seen a fast-paced evolution in the past decade, in virtue of the increased availability of commercial off-the-shelf flight solution suites with high degree of precision and performance at lower costs [6]–[26]. Generally, these systems are additionally equipped with the necessary instrumentation

The associate editor coordinating the review of this manuscript and approving it for publication was Davide Comite.

to record the position of the UAV accurately using on-board GPS and IMU, some form of field strength measurement system (e.g., portable spectrum analyzer, power recorder), and a probe antenna, at the very minimum. Most of these research efforts have been focused in radio astronomy applications operating in VHF bands, although with the advent of 5G technologies, the demand for accurate antenna radiation pattern characterization has increased in microwave telecommunication systems as well, for diagnosing performance, providing adequate coverage, and ensuring standards compliance. As an example in radio astronomy, in 2015, [19] presented a hexacopter system upon which a telescopic dipole is mounted, with the ability to perform measurements of large aperture arrays at frequencies from 50 MHz up to 650 MHz, showing good agreement between simulated and measured co-polarization antenna patterns for E- and H-plane cuts. Later in 2018, [22] presented more results in measuring and validating the 2D radiation pattern of a large ultra wide band array radio telescope; their results found discrepancies in the measured patterns, while highlighting the importance of calibration. In these systems, meeting the FF distance criterion becomes a challenge due to the large aperture sizes; additionally, the antennas under test (AUT) are usually measured in bird-bath mode (i.e., pointed towards zenith) such that there is less contamination from ground reflections. In this context, [21] explored sampling the near field (NF) radiation surrounding the AUT to overcome the FF distance limitations. For telecommunication, [18], [23] and [25] presented a compact, low-cost system for S- and C-bands, capable of centimeter-level accuracy, by sampling the NF (near field) radiation and using a combination phaseless sources reconstruction method and NF-to-FF transformation to obtain the measured FF radiation patterns, with a brief analysis of the impact of the selection of the probe antenna for NF measurements. Then, [26] further improves on these achievements by adding an extra probe and increased positioning accuracy with a dual-band RTK GNSS. A high degree of positioning precision becomes critical at higher operational frequencies, where the errors in position are on the order of a wavelength.

The probe antenna used for characterizing the AUT must also adhere to the strict requirements imposed by the characterization and calibration requirements of the weather radar system. Due to scattering and diffraction effects from the UAV structure (i.e., interaction of the probe antenna and UAV), the radiation characteristics of the probe antenna are degraded. Preliminary results from indoor measurements have shown that said interaction produces ripples in the pattern, which degrades the co-polarization matching between the H- and V-polarizations, and the cross-polarization levels. To adequately calibrate such systems, it is important that these effects are compensated or mitigated. This study attempts to determine to what extent the antenna radiation pattern for different types of antenna is affected by the structure of the UAV focusing on its application in FF (far field) measurements. Additionally, the use of a gimbal as a means to

control the orientation of the probe antenna is also analyzed in this work.

For different antenna types, EM simulations of the probe antenna in free space and mounted on the UAV, which attempt to qualitatively describe the effects of the UAV on the radiation characteristics, are presented in Section II. The simulation performance of each antenna type with respect to the desired standards is presented in Section III. As a means to validate some of the results presented herein, anechoic chamber measurements are presented in Section IV. Finally, a brief discussion summarizing the findings of this work is presented in Section V.

II. SIMULATIONS

A probe antenna that is mounted on a UAV platform for EM field measurements will present radiation characteristics that will be adversely affected by the coupling and scattering effects due to the proximity to its surrounding structure. Moreover, antennas can have different radiation characteristics depending on their type; thus, as the EM fields produced by the antenna interact with the UAV and gimbal structure, they are expected to be correspondingly different. Because of the directional properties and the complex mechanics of this phenomenon, developing accurate analytical models to describe such effects still remain a challenge. In this context, EM simulation software can provide a means to describe such effects with relative accuracy.

A simple model of the UAV platform used for this project [24] is recreated in ANSYS HFSS, and simulated using the finite element method (FEM) and the hybrid method (finite element bounded integral, FE-BI), where the electrically large structure (i.e., UAV and gimbal) is treated with the integral equation method, while the radiating element (i.e., probe antenna) is treated with the FEM method. This decreases the computational complexity of the problem and improves the time taken to complete the simulation, while maintaining an acceptable level of precision. In the following simulated cases, the UAV frame and gimbal are assumed to be leveled with respect to the horizon, stationary, and with the landing gear raised. In other words, the roll, pitch, and yaw angles for both the frame and the gimbal will be 0°. The frequency of the analysis is 3 GHz ($\lambda = 10$ cm) and the antenna types studied are: dipole, microstrip patch, horn, *and patch array*. All cases are presented with the antenna radiation patterns of the antenna in free space and mounted on the UAV, showing the co- and cross-polarized components for H-pol and V-pol in the principal planes (E, D, and H). Additionally, a surface current plot in logarithmic scale is provided to show the region in the UAV and gimbal structure where the currents are more significant (see Figures 1-3). Each case is discussed in the following sections.

A. DIPOLE

For the case of a dipole [27], the radiating element is aligned along the *x*-axis for H-pol (Figure 1a, first column), and along the *y*-axis for V-pol.
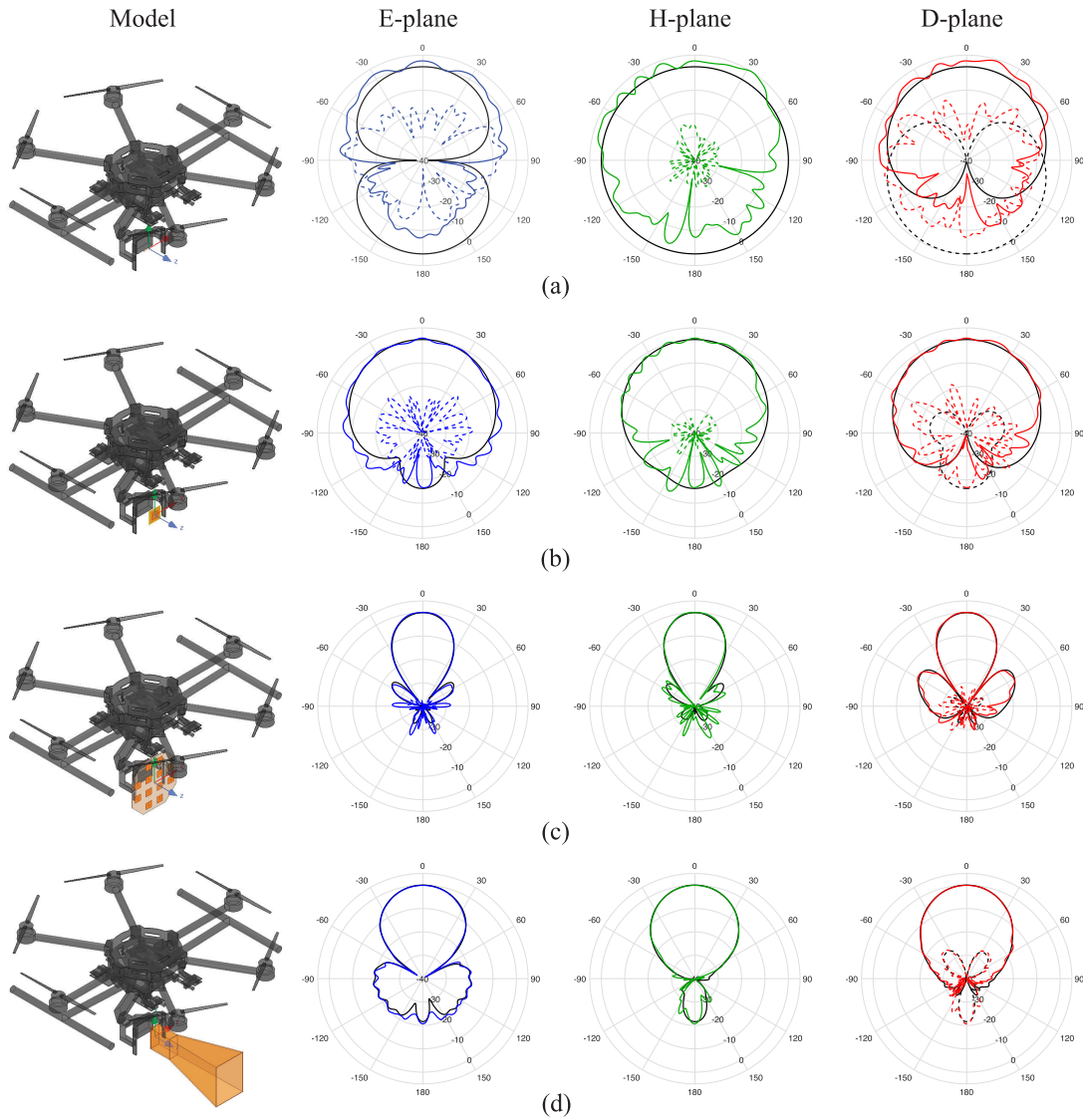
FIGURE 1. H-polarization model of the probe antenna and UAV (first column), and radiation patterns in the E- (second column), H- (third column), and D-planes (fourth column) for: (a) dipole, (b) patch, (c) 4 × 4 array, and (d) horn antenna. Colored lines correspond to the radiation patterns of the probe antenna mounted on the UAV, while black lines correspond to the probe antenna in free space.

The radiation patterns for the E-, H-, and D-planes are shown in Figure 1a second, third, and fourth columns respectively, where the patterns for the dipole in free space are shown in black lines, and for the UAV-mounted in blue, green, and red lines, for the co- (continuous), and cross-polarization (dashed) components. The surface current induced in the UAV structure is shown in Figure 2a.

Clearly, the effect of scattering from the structure can be seen in both co- and cross-polarization patterns in every cut. The co-polarization pattern exhibits ripples about the nominal pattern for the dipole without the UAV, and the cross-polarization pattern increases to approximately -20 dB off boresight, from less than -50 dB. Moreover, it is observed that the increase in the cross-polarization level is less affected in the H-plane. The degradation of the radiation pattern is

quite significant in this case, and it can be hypothesized that the broader the radiation characteristic of the antenna element is, the higher it scatters back from the UAV structure and further contaminates the co- and cross-polarization patterns. Additionally, Figure 2a shows currents being induced more intensely on the gimbal surface than on the UAV frame properly. In this case, the back lobe radiation from the dipole may have a more significant effect in contaminating the antenna radiation patterns than the front lobe radiation.

For V-pol (Figure 3a), the effects are similar but occur at different planes. That is, the co-polarization ripples are higher in the E-plane rather than in the H-plane, as it was in the H-pol case, and the cross-polarization levels are higher in the H-plane, rather than in the E-plane. The surface currents induced in the UAV in this case are more confined within
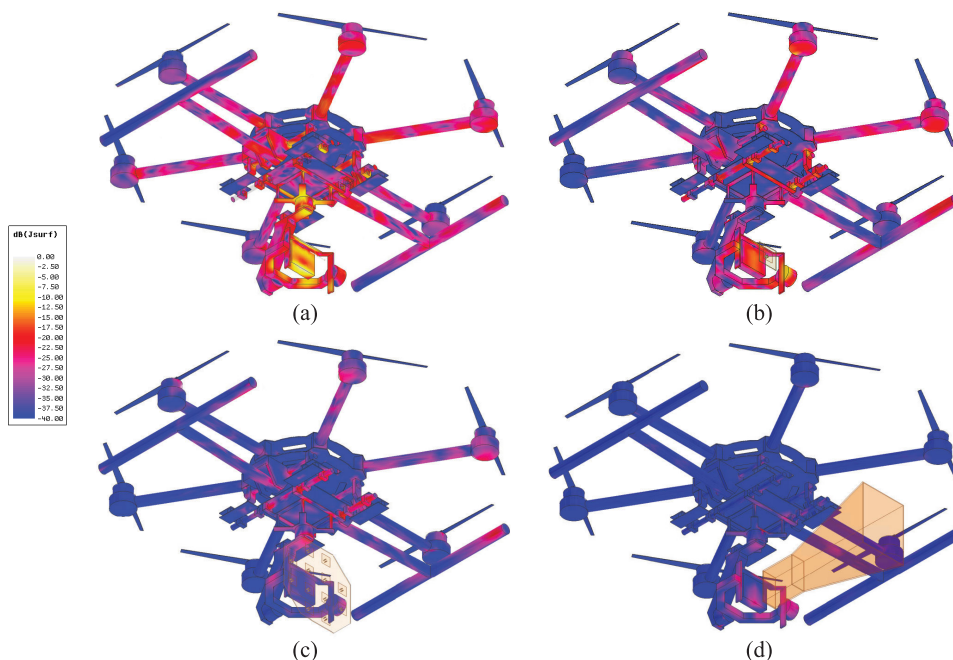
FIGURE 2. H-polarization surface currents induced in the UAV for: (a) dipole, (b) patch, (c) 4 × 4 patch array, and (d) horn antenna.

the gimbal and landing gear region, and not as widespread throughout the frame as it was in the other case.

B. MICROSTRIP PATCH

The microstrip patch antenna [27] analyzed here is dual-polarized and differentially fed (Figure 1b). This antenna in free space exhibits a cross-polarization level less than −40 dB near boresight (Figure 1b). However, when the patch antenna is placed on the UAV and gimbal, the ripples on the co-polarization pattern are relatively weaker compared to the dipole overall, and the cross-polarization level increases near boresight on average by approximately 15 dB in the E-plane, 10 dB in the H-plane, and 20 dB in the D-plane, for H-pol. Notably, the cross-polarization level in the H-plane exhibits a similar behavior as with the dipole case, where it seems less affected than in the other two cuts. This is arguably because the vertical plane is a plane of symmetry for the UAV structure, and therefore, the fields producing such an increment in the cross-polarization level are canceling out. Additionally, the more directive nature of the radiation characteristics in a patch antenna is shown to induce less surface currents in the UAV structure as compared to the case with the dipole, as shown in Figure 2b.

Similar observations made with the dipole in V-pol are made for the patch in V-pol (Figure 3b), where the E-plane co-polarization ripples are higher and cross-polarization levels are lower, and vice versa for the H-plane. This could be attributed to the vertical plane of symmetry, as previously mentioned. Additionally, the surface currents show stronger induced currents in the arms and landing gear of the UAV than it is in H-pol.
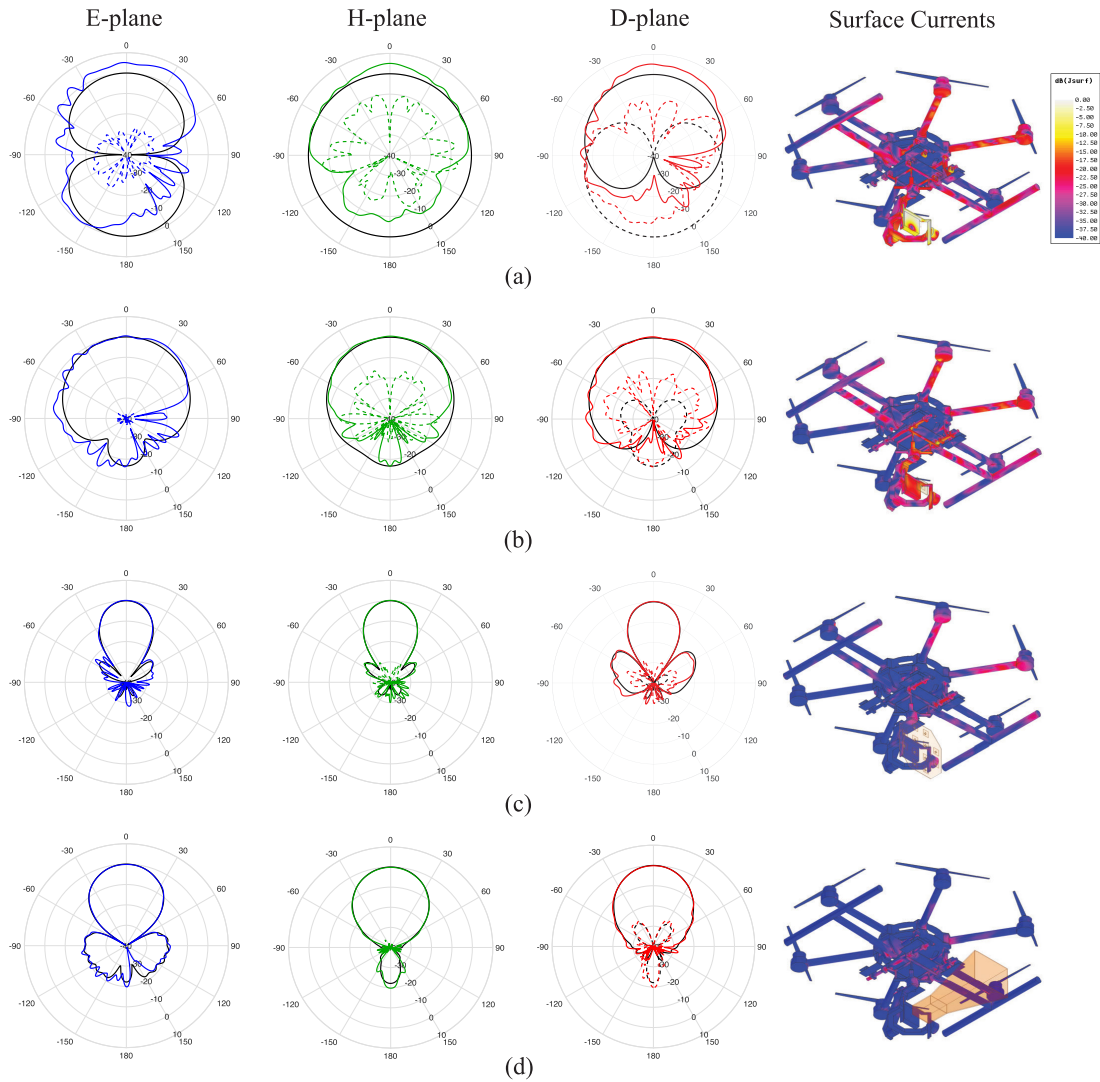
C. PATCH ARRAY ANTENNA

Conducting a similar analysis for a 4 × 4 dual-polarized truncated array [27] (Figure 1c, first column), it can be observed that the radiation pattern of the probe antenna is less distorted by the UAV (Figure 1c, second, third, and fouth columns). However, the co-polarization sidelobe shape is more strongly affected by the ripple effect than near boresight. The higher directivity of this array antenna also shows evidence of less perturbations in the cross-polarization levels, as observed in every cut. For field measurement purposes, this is ideal because the array probe presents a relatively constant amplitude near boresight, and low cross-polarization levels (below −40 dB) as desired. Moreover, the size and weight of the probe allows it to be mounted on a gimbal without having a backlash on the payload of the UAV. Figure 2c also shows less currents induced on the surface of the UAV and the gimbal body, which may explain the better radiation characteristics of this type of probe antenna for UAV applications.

The V-pol E-plane co-polarization pattern (Figure 3c), much like in H-pol H-plane, is slightly asymmetrical compared to the free space radiation pattern. This is effect is less apparent in H-pol E-plane and V-pol H-plane. Aside from that, the cross-polarization levels exhibit similar behavior as with the previous two cases (dipole and patch).

D. HORN

The single-polarized horn antenna [27] model used here resembles those commercially available for RF measurement applications. A caveat here is that this particular scenario has limited applicability in a practical situation due to the weight

E-plane   H-plane   D-plane   Surface Currents

(a)

(b)

(c)

(d)

FIGURE 3. V-polarization radiation patterns in the E- (first column), H- (second column), and D-planes (third column), and surface currents on the UAV for: (a) dipole, (b) patch, (c) 4 × 4 patch array, and (d) horn antenna. Colored lines correspond to the radiation patterns of the probe antenna mounted on the UAV, while black lines correspond to the probe antenna in free space.

and size of the antenna. For example, the use of a S-band horn limits the UAV payload, and it is also difficult to balance the center of gravity of the horn on the gimbal. Nevertheless, if the horn is low-profile and lighter (e.g., a 3D-printed horn antenna), then it becomes feasible for implementation. Referring to Figure 1d, the UAV-mounted horn shows very good radiation characteristics in terms of the ripples in the main lobe, and its cross-polarization levels are virtually unaffected in every plane. Additionally, the surface currents induced on the UAV are the smallest out of the four presented cases, albeit having a slightly wider beamwidth than the array antenna. It can be hypothesized that, in addition to the more directive radiation pattern, the flaring in the horn may provide better shielding from scattering off of the UAV, thus presenting less contamination.

V-pol radiation patterns (Figure 3d), like in H-pol, show little contamination due to the UAV. The most noticeable

change between V-pol and H-pol for the horn is apparent in the surface currents; the gimbal is virtually not inducing any surface currents in V-pol while the lower parts of the frame is, the opposite occurs in H-pol. Nevertheless, the radiation characteristics for the UAV-mounted horn are optimal of all four studied cases.

III. PERFORMANCE ANALYSIS

In the context of antennas for polarimetric weather radar applications, two of the most important requirements are the matching between the co-polarization radiation patterns of the horizontally and vertically polarized (H-, and V-pol, hereafter) channels, and the cross-polarization levels in both H-pol and V-pol. However, it is no trivial task to evaluate the performance of a probe antenna mounted on a UAV, as the effects of their interaction can be difficult to predict. To facilitate this, analysis metrics that highlight certain

aspects of these effects are used in this study, which include co-polarization mismatch, ripples in H- and V-pol, maximum cross-polarization level, and the ratio between the cross-polarized energy of the UAV-mounted antenna and in free-space; they are described next.

A. DESCRIPTION OF METRICS

1) CO-POLARIZATION MISMATCH

The co-polarization mismatch between the H- and V-channels as a function of the direction is defined as:

$$M_{HV}(\theta, \phi) = F_H^{co}(\theta, \phi) - F_V^{co}(\theta, \phi) \tag{1}$$

expressed in dB,[1] where F_H^{co} is the co-polarized H-pol radiation pattern, F_V^{co} is the co-polarized V-pol radiation pattern in their corresponding planes of polarization given by ϕ, respectively.[2] While (1) generalizes the co-polarization mismatch for all directions, the most important one for these analyses is in the scanning angle or boresight direction, which will be denoted by as θ_0 (e.g., $M_{HV}(\theta_0, \phi)$).

Additionally, it is assumed that during an actual in-situ measurement operation, the beam of the probe antenna will remain relatively aligned with the desired direction; thus, a region of interest can be defined to simplify the analysis. Here, the region within the 3-dB beamwidth θ_3 will be used to analyze the performance of the metrics under study. In other words, the range of θ values for the analyses will usually be assumed to be

$$\theta_0 - \frac{\theta_3}{2} \leq \theta \leq \theta_0 + \frac{\theta_3}{2} \tag{2}$$

unless otherwise specified.

2) RIPPLES

To calculate the ripple level due to coupling and scattering off of the UAV structure for each polarization channel, the mounted probe's radiation pattern needs to be compared to a comparable reference. For this, the pattern of the probe in free space is subtracted from the composite probe-and-UAV pattern as:

$$\Delta_x(\theta) = F_{x,u}^{co}(\theta, \phi)\big|_{\phi=\phi_0} - F_{x,a}^{co}(\theta, \phi)\big|_{\phi=\phi_0}, \tag{3}$$

where x can be H or V depending on the polarization and ϕ_0 is the desired cut.[3] From (3), the standard deviation (for logarithmic variables) is calculated across θ, denoted by the $\sigma[\cdot]$ operator; e.g., $\sigma[\Delta_H]$, where the angular dependency has been ignored for simplicity.

This metric measures the variability in the H-pol and V-pol co-polarization radiation patterns added by undesired reflections from the UAV within the angular range of interest. The

---

[1]Uppercase variable notation will generally be used to denote variables in dB, while lowercase will be used for linear units.

[2]The coordinate system and polarizations are usually defined in Ludwig-III.

[3]The subscripts a and u will be used throughout the text to refer to the radiation pattern of the antenna without and with the UAV structure, respectively, where needed.

principal planes (cuts) of polarization, E, D, and H will be studied here, which correspond to ϕ_0 values of 0°, 45°, and 90°, respectively.

A similar definition can be made for the cross-polarization ripples, although owing to its somewhat unpredictable nature and very low levels (i.e., less than -30 dB), an extremely high precision for the relative error in the simulations (and in measurements) would be required and thus is not included in the analysis.

3) CROSS-POLARIZATION METRICS

For weather radar applications, one of the two key aspects is achieving a very low cross-polarization level. Cross-polarization radiation is predominantly affected by scattering and depolarizing mechanics due to the presence of the UAV. It is inherently difficult to quantify such effects; however, the maximum cross-polarization level and the ratio of the cross-polarized energy (between UAV-mounted and free-space probe cases) can provide a means to quantify them.

The maximum in the cross-polarization radiation pattern is normalized with respect to the co-polarization boresight as:

$$MXL = \max_\theta F_x^{cx}(\theta, \phi)\big|_{\phi=\phi_0} - F_x^{co}(\theta_0, \phi)\big|_{\phi=\phi_0}, \tag{4}$$

where the local maximum is computed for the range of interest θ and for the given ϕ_0 cut.

The ratio of the cross-polarized energy that is scattered in the region of interest by the probe antenna with the UAV with respect to free space (XER) is calculated as:

$$XER = 10\log_{10}\left(\frac{\int |f_{x,u}^{cx}(\theta, \phi)|^2 d\theta\big|_{\phi=\phi_0}}{\int |f_{x,a}^{cx}(\theta, \phi)|^2 d\theta\big|_{\phi=\phi_0}}\right), \tag{5}$$

and it represents the increase in cross-polarization energy of the probe antenna when in presence of the UAV, for the θ range of interest.

B. ANALYSIS

In this section, a performance analysis will be provided based on the radiation characteristics presented in Section II and the metrics [(1)-(5)] previously discussed. For the sake of brevity, the analysis will focus on the E-plane radiation patterns, although similar analysis can be made in any other cut of interest.

1) DIPOLE

The dipole radiation patterns in E-plane is a particular case due to the broad radiation characteristics that presents. The region where the gain is greater than 3-dB consists of a front lobe and a back lobe. As a result of this, it can be predicted that the fields scattered from the structure will have a stronger impact both in the co- and cross-polarization radiation patterns, as previously discussed. The region of interest in this case becomes anywhere where the gain is greater than 3 dB, and plots corresponding to the metrics of interest are shown in Figure 4. The co-polarization mismatch for the dipole is shown in Figure 4a, with the boresight values (marked) of
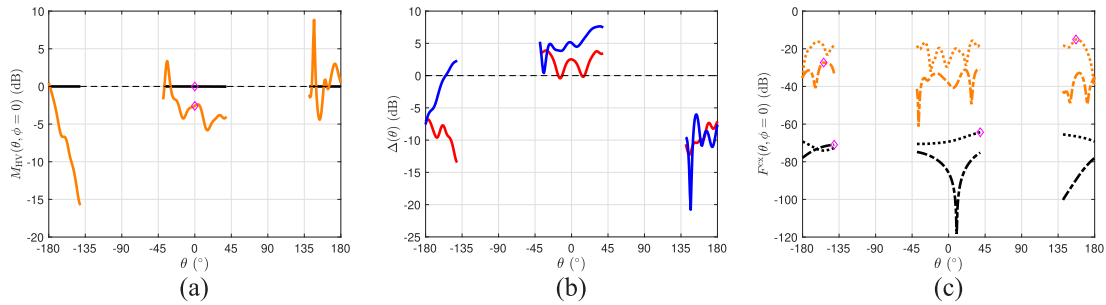
FIGURE 4. Performance of the simulated dipole in terms of: (a) co-polarization mismatch for free space (black) and mounted on the UAV (orange), (b) H- (red) and V-pol (blue) ripples in co-polarization pattern, and (c) cross-polarization patterns of free space (black) and mounted on UAV (orange) for H- (dotted) and V-pol (dash-dotted).
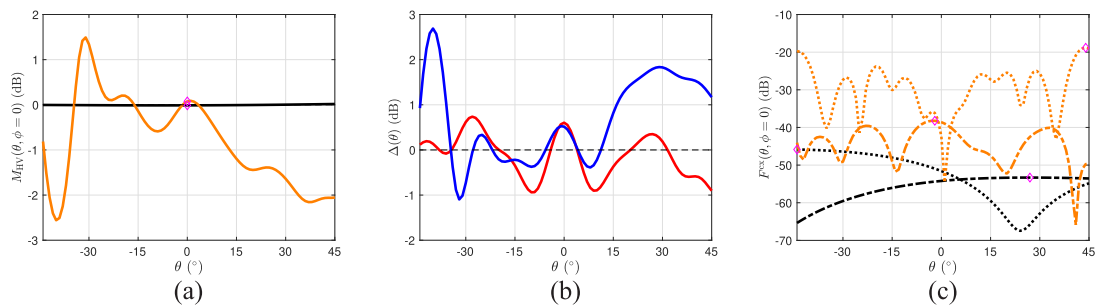
FIGURE 5. Performance of the simulated patch in terms of: (a) co-polarization mismatch for free space (black) and mounted on the UAV (orange), (b) H- (red) and V-pol (blue) ripples in co-polarization pattern, and (c) cross-polarization patterns of free space (black) and mounted on UAV (orange) for H- (dotted) and V-pol (dash-dotted).

−0.01 dB and −2.59 dB for the probe in free space and on the UAV, respectively. Outside of boresight, these values change rapidly on the UAV, so ideally it should be required that the probe orientation relative to the nose of the UAV be very small (or known and constant) such that appropriate corrections can be applied. Nevertheless, the standard deviation of the mismatch in this range is 0.006 dB in free space and 2.628 dB on the UAV, which does not meet the 0.1 dB requirement for weather radar applications.

By normalizing the free-space radiation pattern to the UAV-mounted pattern, it is possible to visualize the net effect of adding the UAV into the testing environment. The ripples in the co-polarization patterns added due to the presence of the UAV with respect to the free space pattern are plotted in Figure 4b for the H- (red) and V-pol (blue) cases. Obviously, the effect of the ripples is to add uncertainties in the mismatch between the co-polarization patterns. The standard deviation for the mismatch in H-pol is 3.51 dB and in 4.64 dB in V-pol. This illustrates the fact that a dipole used as a probe for UAV-based antenna measurements would be less than ideal for this application.

The cross-polarization patterns for the free space and UAV cases are shown in Figure 4c, where the maximum of each is marked. The maximum levels in free space are found to be −64.33 dB and −70.98 for the H- and V-pol, respectively, whereas on the UAV they increase to −15.06 dB and −27.31 dB. This yields an increase of approximately 50 dB in H-pol and 44 dB in V-pol, which is quite significant. As an

additional measure, using (5) the ratio of the cross-polarized energy radiated with the UAV with respect to free space is found to be 51.53 dB for H-pol and 48.44 dB for V-pol.[4]
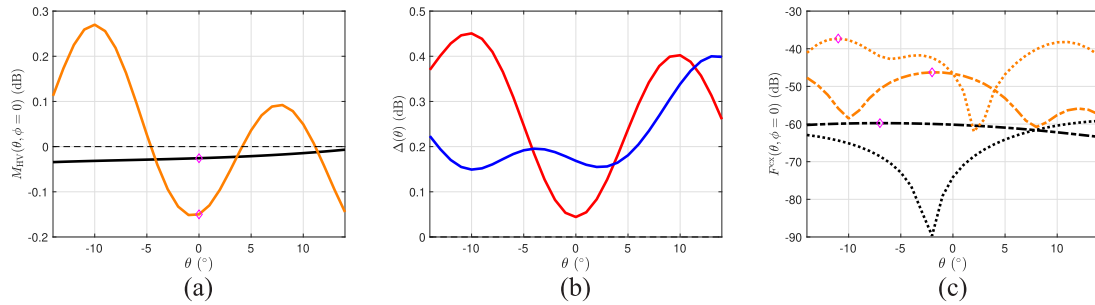
2) PATCH

A similar analysis is done for the patch antenna, which exhibits a more directive radiation pattern than the dipole, with a 3-dB beamwidth of approximately 90°. It can be predicted that, with the back lobe radiation being weaker for this case, the contamination from the UAV structure would be smaller.
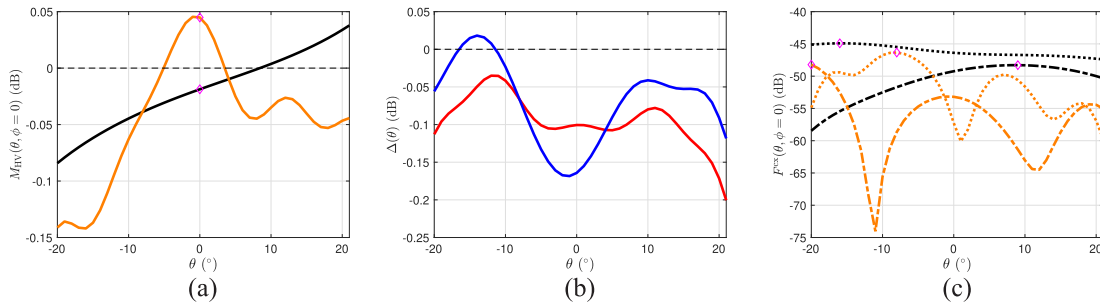
The co-polarization mismatch (Figure 5a) shows boresight values of −0.01 dB and 0.07 dB for the probe in free space and on the UAV, respectively. The variability of the mismatch is smaller, with the standard deviation being 0.008 dB in free space and 0.878 dB on the UAV. The mismatch characteristics show an improvement of about 2 dB on the UAV when compared to the dipole case, though still above the desired level. The ripples in the co-polarization patterns are plotted in Figure 5b for H- (red) and V-pol (blue). The standard deviation for the mismatch in H-pol is 0.45 dB and 0.97 dB in V-pol. The patch antenna exhibits less ripples in the main beam in both H- and V-pol cases, and a better performance overall than the dipole.

The maximum levels in the cross-polarization patterns (Figure 5c) in free space are found to be −45.86 dB and

---

[4]In other words, the cross-polarization power is approximately 100,000 times higher when mounted on the UAV!

FIGURE 6. Performance of the simulated 4 × 4 patch array in terms of: (a) co-polarization mismatch for free space (black) and mounted on the UAV (orange), (b) H- (red) and V-pol (blue) ripples in co-polarization pattern, and (c) cross-polarization patterns of free space (black) and mounted on UAV (orange) for H- (dotted) and V-pol (dash-dotted).

FIGURE 7. Performance of the simulated horn in terms of: (a) co-polarization mismatch for free space (black) and mounted on the UAV (orange), (b) H- (red) and V-pol (blue) ripples in co-polarization pattern, and (c) cross-polarization patterns of free space (black) and mounted on UAV (orange) for H- (dotted) and V-pol (dash-dotted).

−53.32 for the H- and V-pol, respectively, whereas on the UAV they increase to −18.83 dB and −38.23 dB, yielding an increase of approximately 27 dB in H-pol and 15 dB in V-pol and showing an improvement over the dipole case. The ratio of the cross-polarized energy radiated with the UAV with respect to free space is 23.99 dB for H-pol and 12.73 dB for V-pol.

3) ARRAY

The array design used in this study has a 3-dB beamwidth of approximately 28°, as shown in Figure 1c for H-pol and Figure 3c for V-pol. An improvement in the metrics with respect to the previous cases is immediately apparent; although, it should be noted that a narrower beamwidth probe antenna is more vulnerable to errors due to stability of the UAV and relative alignment between the probe and the UAV. The mismatch at boresight is shown in Figure 6a to be −0.03 dB in free space and −0.15 dB on the UAV, with a standard deviation of 0.01 dB and 0.13 dB respectively, which approximately meets the requirement of 0.1 dB. Such performance can be improved if the variation of the relative alignment between the UAV and the probe is sufficiently small (i.e., within a few degrees off boresight).

The amplitude of the ripples in both polarizations (Figure 6b) is also notably smaller than in the previous cases, showing how an array probe would be less vulnerable to variations in co-polarization mismatch due to probe-UAV misalignment. The standard deviation of the ripples are 0.14 dB in H-pol and 0.08 dB in V-pol.

Figure 6c shows the maximum cross-polarization levels in free space to be −59.17 dB and −59.76 dB for H- and V-pol,

respectively, and, analogously −37.29 dB and −46.26 dB on the UAV, for a total increase of approximately 22 dB in the H-pol and 14 dB in the V-pol cross-polarization levels. As previously mentioned, this performance can be improved by constraining the relative alignment between the probe and UAV to within a few degrees from boresight. While the ability to measure normalized cross-polarization levels down to −50 dB is sought after ideally, −35 to −40 dB is usually sufficient for the application. The XER in the H-pol is 23.19 dB and 10.47 dB in V-pol.

4) HORN

The horn analyzed here presents a special case because the radiation pattern shows a 3-dB beamwidth of approximately 41°, which is wider than the array, and also shows a slightly higher back lobe radiation than the array. Nevertheless, the metrics show a comparable or even better performance than the array in some cases. It is hypothesized that the flaring of the horn antenna allows a degree of shielding from the backscattered radiation off of the UAV structure, and thus, the mismatch, ripples, and cross-polarization levels have better performances overall. Figure 7a shows the co-polarization mismatch for the horn in free space and with the UAV, with the values in boresight of −0.02 dB and 0.05 dB respectively, and the standard deviations are calculated as 0.03 dB and 0.05 dB.

The ripples in H- and V-pol for the horn are the smallest yet, with standard deviations of the amplitudes of 0.03 dB and 0.05 dB respectively, showing the best performance over a wider range of angles.

TABLE 1. Summary of relevant performance metrics.

	Dipole	Patch	Array	Horn
Weight (kg)	< 0.1	0.2	0.9	3.0
Endurance (min)	30	29	25	18
$\sigma[M_{\mathrm{HV,u}}]$ (dB)	2.63	0.88	0.13	0.05
$\sigma[\Delta_{\mathrm{H}}]$ (dB)	3.51	0.45	0.14	0.03
$\sigma[\Delta_{\mathrm{V}}]$ (dB)	4.63	0.97	0.08	0.05
$\mathrm{MXL}_{\mathrm{H,u}}$ (dB)	-15.06	-18.83	-37.29	-46.34
$\mathrm{MXL}_{\mathrm{V,u}}$ (dB)	-27.31	-38.23	-46.26	-48.22
$\mathrm{XER}_{\mathrm{H}}$ (dB)	51.53	23.99	23.19	-4.52
$\mathrm{XER}_{\mathrm{V}}$ (dB)	48.44	12.73	10.57	-5.07

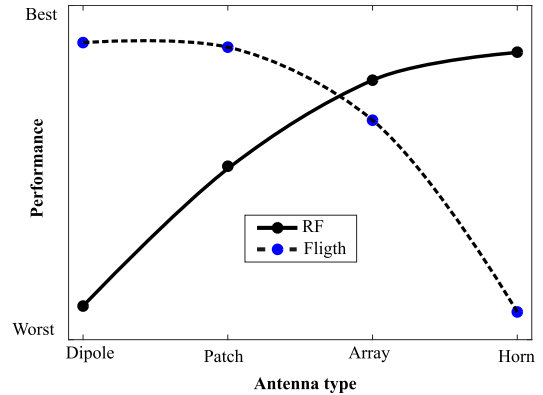**FIGURE 8.** Qualitative flight and RF performances for different antenna types.

Although in free space, the maximum cross-polarization levels of the horn radiation patterns in H- and V-pol are not lower than the array's, at -44.91 dB for H-pol and -48.91 dB for V-pol, when mounted on the UAV, these levels remain virtually the same. On the UAV, the maximum levels are found to be -46.34 dB for H-pol and -48.22 dB for V-pol, with a relative difference of approximately 1.4 dB and 0.07 dB respectively. The XER for the H-pol case yields -4.52 dB for H-pol and -5.07 dB for V-pol, indicating that the cross-polarization energy being radiated is the smallest for the horn than the rest of the cases.

C. PROBE SELECTION

The best probe antenna for the application should ideally meet the RF performance criteria while being able to sustain flight endurance long enough to complete an operation uninterrupted. Typical values for the weights of the studied antennas and the UAV endurance with the antennas mounted on are presented in Table 1, based on the platform that has been used for testing [24]. Additionally, the metrics that are most relevant to the RF performance of the probe and UAV set are listed in Table 1 for each case in the E-plane.

The endurance is directly related to flight performance, i.e., longer endurance is better, and the factors that affect it are the takeoff and payload weight, payload placement within the UAV frame, the flight strategy to be conducted, etc. The co-polarization mismatch is inherently related to the radiation characteristics for each polarization channel (H or V), and is additionally affected by the ripples in the respective channel. Ideally, the mismatch should be zero; thus, lower mismatch and ripples result in better RF measurement performance. On the other hand, the energy radiated in the cross-polarization should ideally by zero (or infinity in dB) producing less distortion in the cross-polarization patterns when mounted on the UAV; i.e., less is better. As such, a maximum cross-polarization level of approximately -50 dB or better is sought after ideally.

Based on Table 1, and by assigning weights to these parameters, it is possible to qualitatively determine their performance according to the best and worst cases between
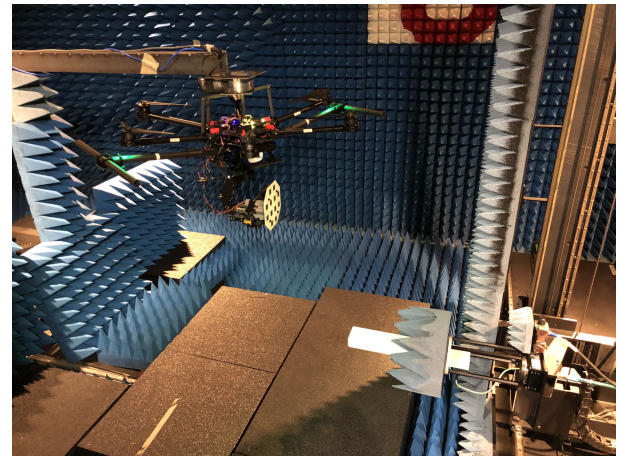

FIGURE 9. Measurement setup in planar near-field anechoic chamber: UAV with landing gear in engaged position with probe antenna (4 × 4 patch array) mounted on gimbal. The measurements were performed in the NF (pictured above) and FF anechoic chamber facilities of the University of Oklahoma's (OU) Advanced Radar Research Center (ARRC).

the four antenna types analyzed. Such depiction is shown in Figure 8, where the RF performance (black) is overlaid with the flight performance (blue). This representation shows the trade-off between the UAV endurance and payload versus the desired RF measurement performance criteria. The analysis presented in this section shows the dipole and horn having the worst and best RF performance respectively, while simultaneously having the best and worst flight performance. There is a marginal improvement in going from an array to a horn in terms of RF performance, while the loss in flight performance is quite significant. Similarly, while there is a slight improvement in endurance going from an array to a patch, the loss in RF performance is such that the minimum requirements are harder to achieve. Therefore, the array is selected as the probe antenna to be mounted on the UAV, since it has the best performance overall, when RF and flight performances are taken into account.

IV. MEASUREMENTS

In this section, indoor characterization of the array antenna mounted on the UAV is presented, and the variability of the radiation patterns due to the relative alignment of the probe
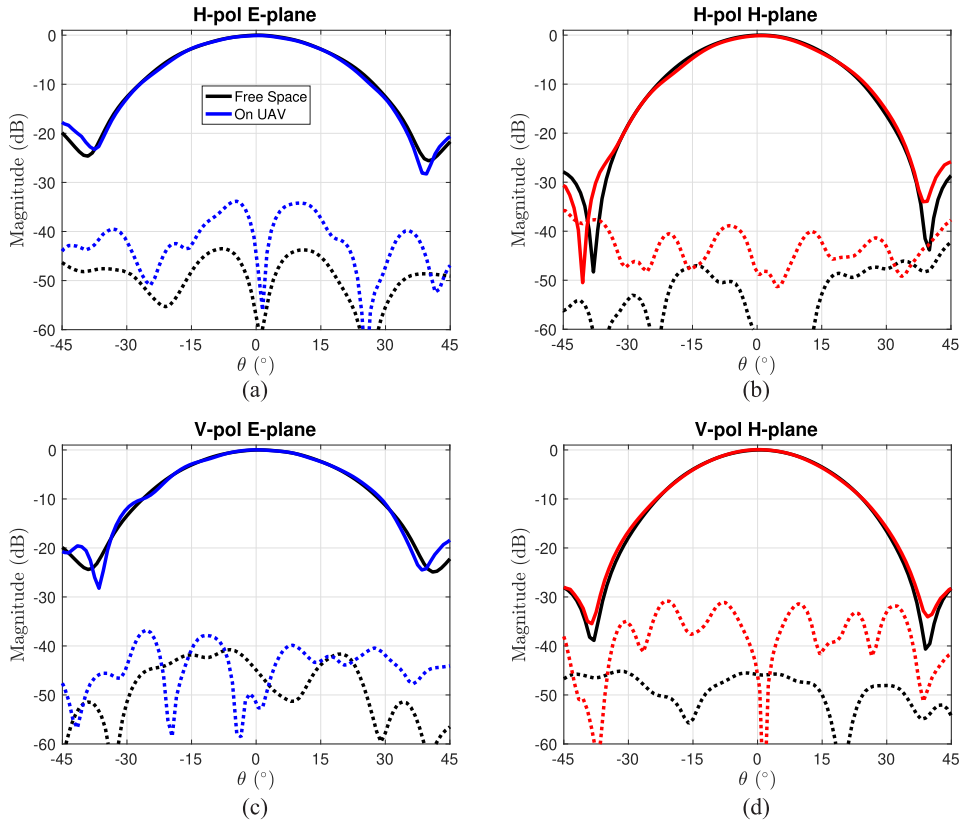
FIGURE 10. Normalized measured antenna radiation patterns of the truncated 4 × 4 patch array antenna used as a probe in free space (black) and mounted on the UAV (blue/red) for: (a) H-pol, E-plane, (b) H-pol, H-plane, (c) V-pol, E-plane, and (d) V-pol, H-plane.
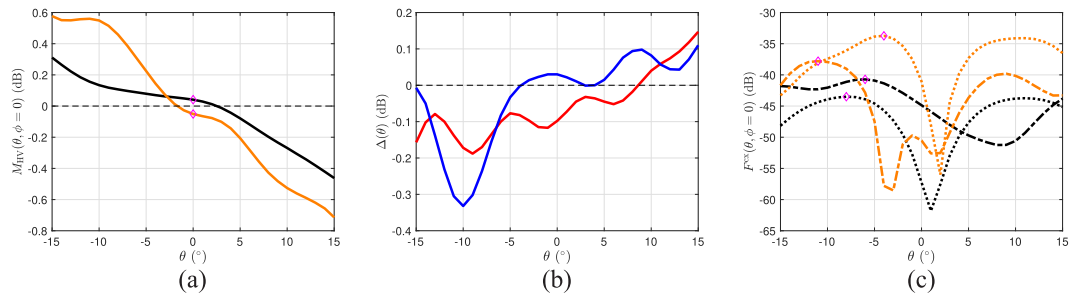
FIGURE 11. Performance of the measured array in terms of: (a) co-polarization mismatch for free space (black) and mounted on the UAV (orange), (b) H- (red) and V-pol (blue) ripples in co-polarization pattern, and (c) cross-polarization patterns of free space (black) and mounted on UAV (orange) for H- (dotted) and V-pol (dash-dotted). The gimbal orientation angles are α_r, α_p, $\alpha_y = 0°$ relative to the UAV frame.

and the UAV frame is also studied. The measurements were performed at the University of Oklahoma's Advanced Radar Research Center (ARRC) facilities (Fig. 9).

A. FOLLOW MODE

When the UAV is hovering about a point in space while the AUT is being measured, it is desirable that the probe antenna has no relative orientation difference with respect to the nose of the UAV to keep the variance in measurement to a minimum. In the gimbal's follow operating mode, the probe antenna follows the nose of the UAV, and there is no relative movement between the UAV and the probe antenna, which is similar to the configurations used in the simulations from previous sections.

To validate the simulations of Section II-C, indoor measurements of the array antenna in free space and mounted on the UAV are taken in H- and V-polarizations, for E- and H-planes (Fig. 10).

For the most part, the simulations and measurements are in good agreement, with inherent discrepancies that can be attributed to the uncertainty in the measurement process, as well as tolerances and faults in the fabrication process. More importantly, the distortion in the radiation patterns due to the presence of the UAV is congruent, as it is noticeable in the V-pol E-plane, and in the H-planes for both polarizations. On the other hand, the increase in the cross-polarization level is also apparent in the measurements, albeit a couple of dB higher than in the simulations.
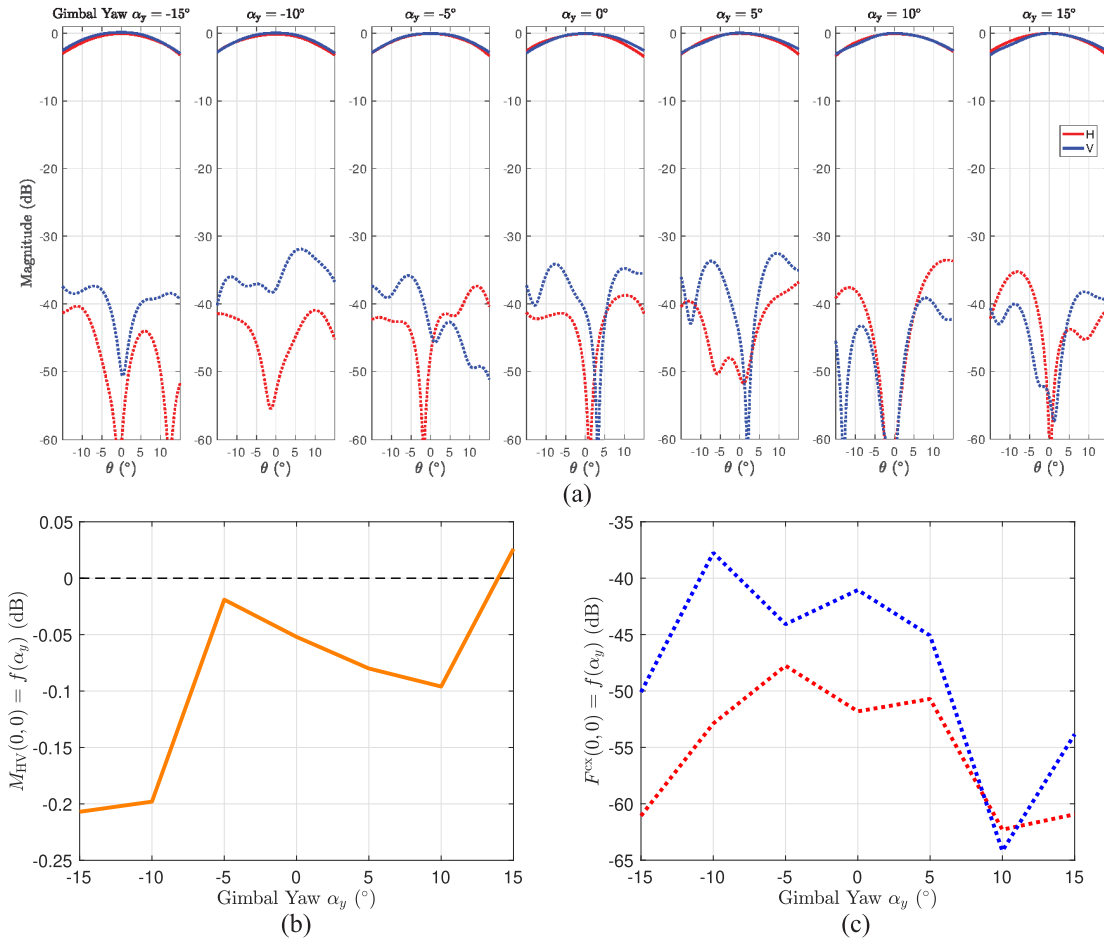
FIGURE 12. Radiation characteristics of the probe antenna mounted on the UAV and gimbal: (a) radiation patterns in co-(solid) and cross-polarizarion (dashed), for H- (red) and V-pol (blue), for different gimbal yaw angles relative to the nose of the UAV, (b) mismatch at boresight (0° for each pattern in (a)) between H- and V-pol, and (c) cross-polarization levels at boresight (same as (b)) for H- (red) and V-pol (blue).

The metrics calculated for the measurements are shown in Fig. 11. From Fig. 11a and b, the effect of the ripples due to the UAV frame is evident, as it was in the simulations. The mismatch at boresight (Fig. 11a) is measured at 0.04 dB for free space and −0.05 dB on the UAV, which meets the requirement of 0.1 dB. The standard deviation for the mismatch in the 3-dB beamwidth range is 0.20 dB in free space and 0.43 dB on the UAV, which can be improved as long as the gimbal and the UAV are stable enough within a few degrees off boresight when pointing towards the AUT. The H- and V-pol ripples (Fig. 11b) are measured with a standard deviation of 0.08 dB and 0.12 dB respectively.

The maximum cross-polarization levels (Fig. 11c) in H-pol are measured at −43.50 dB and −33.74 dB in free space and on the UAV, respectively, while in V-pol, they are −40.72 dB and −37.80 dB. From these numbers, the increase in the cross-polarization level due to the presence of the UAV is approximately 10 dB in H-pol and 3 dB in V-pol. Although the cross-polarization measurements are expected to be higher than the simulations, the higher increase in H-pol than in V-pol is in agreement with the simulations. Additionally, the maxima in the cross-polarization levels are located far

from boresight, so the performance can be increased if the range of operation is limited, as discussed previously.

B. TRACKING MODE

When the flight strategy is not hovering mode, the use of a gimbal adds additional degrees of freedom for the probe antenna to be aligned with the phase center of the AUT. For this study, only the yaw angle of the gimbal is varied and characterized indoors; however, it should be noted that the roll and pitch angles may vary as well, and as such, it is desired to keep them stable about zero degrees to avoid displacement of boresight and measurement planes.

The probe antenna is then characterized in chamber (Fig. 12) by maintaining the gimbal and probe antenna aligned while varying the yaw angle of the UAV frame between −15° and 15°.[5]

At the angles of ±10° and ±15°, the mismatch and cross-polarization levels vary significantly from those at

---

[5]This set of measurements is different from the ones in the previous section, and due to alignment and other factors, the V-pol pattern is somewhat different at a gimbal yaw angle of zero, though other characteristics remain unchanged.

0° gimbal yaw, while between −5° and 5° the variance is tolerable. This supports the idea that by limiting the operating range of gimbal yaw angles, the effects of the UAV on the radiation characteristics of the probe antenna can be mitigated to some extent, and also provides an insight on how the probe antenna behaves as a function of its orientation relative to the UAV frame.

V. CONCLUSION
In the selection of an optimal probe antenna for polarimetric weather radar characterization using UAVs, some factors have to be considered. One of the most important is the degradation of the radiation characteristics of the probe antenna due to being in the proximity of the UAV frame. Different types of antennas will present different behavior due to their inherent radiation characteristics, and therefore the scattering from the UAV will be different; thus, it is important to understand this behavior such that the probe antenna can be adequately selected. It is emphasized that this application imposes strict requirements in terms of co-polarization mismatch levels and maximum cross-polarization levels, in the order of 0.1 dB and approximately −40 dB, respectively. These restrictions may be relaxed depending on the operational mode, but it is the standard that guarantees low biases in the polarimetric weather radar products.

The effects of scattering due to the proximity of the UAV frame to the probe antenna have been investigated in this work through simulations and validated with measurements in the appropriate scenarios. The simulated radiation patterns have shown the effect of the ripples being added on the co-polarization radiation patterns and an increase in the cross-polarization levels. According to the metrics presented in Section III, the dipole has shown the worst RF performance, and the horn the best performance. Conversely, the horn has shown the worst flight performance, whereas the dipole is the lightest of antenna types, thus having the best fight performance. However, when taking into account both RF and flight performances, the array is found to be the best candidate for this application owing to its light weight, low-profile, and acceptable RF performance. Nevertheless, the horn-type of antennas would be ideally preferred, as the surface current plots show minimal scattering off the UAV frame, and less contamination in the radiation patterns. The downside of a high-precision horn is their weight and the profile which would imbalance the weight distribution on the gimbal and degrade the endurance of the UAV; an alternative that could be further explored is a horn antenna made of light-weight materials that would overcome the limitations.

Additionally, the simulated array case has been validated with anechoic chamber measurements, where the effect of scattering from the UAV has been shown to be in qualitative agreement. The ripples and the increment in the cross-polarization levels have shown a similar behavior both in measurements as in simulations, with an increase in the cross-polarization level of approximately 3 to 10 dB in the UAV with respect to the probe antenna in free space.

Furthermore, the variance of the radiation patterns as the yaw angle of the gimbal is varying (i.e., change in the relative alignment between the probe antenna and the UAV nose) has been studied. Based on the results, it is recommended that the range of operation of the gimbal yaw should be limited to within a few degrees off from the nominal zero degree (no misalignment with respect to the UAV) to have an RF performance that is still within the required limits. In this case, the variance is not significant as long as the gimbal is operating within −5° and 5°. It is important to note that the variance due to the roll and pitch angles have not been included in this study, and it could be a considerable source of error and should not be disregarded.

In summary, the simulations and measurements have shown a good agreement with regards to the effect of scattering due to the proximity and relative orientation of the UAV and the probe antenna; and the EM simulation can be an useful tool to determine the performance of the system before final implementation. The array antenna studied for this project, as a baseline, is found to be in agreement with the requirements for polarimetric weather radar characterization. Further strategies to improve the quality of the measurements can be based in the design of the antenna itself, or by implementing signal processing techniques either during flight or in post-processing.

REFERENCES
[1] J. E. Stailey and K. D. Hondl, "Multifunction phased array radar for aircraft and weather surveillance," *Proc. IEEE*, vol. 104, no. 3, pp. 649–659, Mar. 2016.

[2] I. R. Ivić, "An approach to simulate the effects of antenna patterns on polarimetric variable estimates," *J. Atmos. Ocean. Technol.*, vol. 34, no. 9, pp. 1907–1934, Sep. 2017.

[3] C. Fulton, J. Salazar, D. Zrnic, D. Mirkovic, I. Ivic, and D. Doviak, "Polarimetrie phased array calibration for large-scale multi-mission radar applications," in *Proc. IEEE Radar Conf. (RadarConf)*, Apr. 2018, pp. 1272–1277.

[4] "IEEE standard test procedures for antennas," Inst. Elect. Electron. Eng. (IEEE), Piscataway, NJ, USA, Tech. Rep., 1979, vol. 149, no. 1979.

[5] J. S. Hollis, T. Lyon, and L. Clayton, *Microwave Antenna Measurements*. San Jose, CA, USA: Scientific-Atlanta, 1970.

[6] G. Virone, A. M. Lingua, M. Piras, A. Cina, F. Perini, J. Monari, F. Paonessa, O. A. Peverini, G. Addamo, and R. Tascone, "Antenna pattern verification system based on a micro unmanned aerial vehicle (UAV)," *IEEE Antennas Wireless Propag. Lett.*, vol. 13, pp. 169–172, 2014.

[7] G. Virone, F. Paonessa, O. A. Peverini, G. Addamo, R. Orta, R. Tascone, A. Lingua, M. Piras, P. Bolli, G. Pupillo, and J. Monari, "Antenna pattern measurement with UAVs: Modeling of the test source," in *Proc. 10th Eur. Conf. Antennas Propag. (EuCAP)*, Apr. 2016, pp. 1–3.

[8] F. Paonessa, G. Virone, P. Bolli, G. Pupillo, J. Monari, F. Perini, A. Mattana, G. Naldi, M. Poloni, M. Schiaffino, A. M. Lingua, M. Piras, P. Dabove, I. Aicardi, G. Addamo, O. A. Peverini, R. Orta, and R. Tascone, "The UAV-based test source as an end-to-end verification tool for aperture arrays," in *Proc. Int. Conf. Electromagn. Adv. Appl. (ICEAA)*, Sep. 2016, pp. 886–889.

[9] F. Paonessa, G. Virone, E. Capello, G. Addamo, O. A. Peverini, R. Tascone, P. Bolli, G. Pupillo, J. Monari, M. Schiaffino, F. Perini, S. Rusticelli, A. M. Lingua, I. Aicardi, and P. Maschio, "VHF/UHF antenna pattern measurement with unmanned aerial vehicles," in *Proc. IEEE Metrol. Aerosp. (MetroAeroSpace)*, Jun. 2016, pp. 87–91.

[10] F. Paonessa, G. Virone, I. Aicardi, A. M. Lingua, M. Piras, P. Maschio, P. Bolli, G. Addamo, O. A. Peverini, R. Orta, and R. Tascone, "Recent results in antenna pattern measurement with UAVs," in *Proc. Int. Conf. Electromagn. Adv. Appl. (ICEAA)*, Sep. 2015, pp. 720–721.

[11] G. Virone, F. Paonessa, E. Capello, O. A. Peverini, G. Addamo, R. Tascone, R. Orta, M. Orefice, A. Lingua, M. Piras, I. Aicardi, P. Bolli, J. Monari, F. Perini, G. Pupillo, and M. Schiaffino, "UAV-based antenna and field measurements," in *Proc. IEEE Conf. Antenna Meas. Appl. (CAMA)*, Oct. 2016, pp. 1–3.

[12] G. Virone, F. Paonessa, O. A. Peverini, G. Addamo, R. Orta, R. Tascone, and P. Bolli, "Antenna pattern measurements with a flying far-field source (hexacopter)," in *Proc. IEEE Conf. Antenna Meas. Appl. (CAMA)*, Nov. 2014, pp. 1–2.

[13] G. Virone, F. Paonessa, A. Tibaldi, Z. Farooqui, G. Addamo, O. A. Peverini, R. Tascone, P. Bolli, A. Mattana, J. Monari, G. Naldi, F. Perini, G. Pupillo, M. Schiaffino, A. M. Lingua, M. Piras, P. Maschio, I. Aicardi, I. H. Bendea, and A. Cina, "UAV-based radiation pattern verification for a small low-frequency array," in *Proc. IEEE Antennas Propag. Soc. Int. Symp. (APSURSI)*, Jul. 2014, pp. 995–996.

[14] F. Paonessa, G. Virone, G. Addamo, O. A. Peverini, R. Tascone, E. D. L. Acedo, E. Colin-Beltran, N. Razavi-Ghods, P. Bolli, G. Pupillo, G. Naldi, J. Monari, A. M. Lingua, M. Piras, I. Aicardi, and P. Maschio, "UAV-based pattern measurement of the SKALA," in *Proc. IEEE Int. Symp. Antennas Propag. USNC/URSI Nat. Radio Sci. Meeting*, Jul. 2015, pp. 1372–1373.

[15] F. Ustuner, E. Aydemir, E. Gulec, M. Ilarslan, M. Celebi, and E. Demirel, "Antenna radiation pattern measurement using an unmanned aerial vehicle (UAV)," in *Proc. 31st URSI Gen. Assem. Sci. Symp. (URSI GASS)*, Aug. 2014, pp. 1–4.

[16] A. M. Picar, C. Marque, M. Anciaux, H. Lamy, and S. Ranvier, "Antenna pattern calibration of radio telescopes using an UAV-based device," in *Proc. Int. Conf. Electromagn. Adv. Appl. (ICEAA)*, Sep. 2015, pp. 981–984.

[17] S. Duthoit, J. L. Salazar, W. Doyle, A. Segales, B. Wolf, C. Fulton, and P. Chilson, "A new approach for *in-situ* antenna characterization, radome inspection and radar calibration, using an unmanned aircraft system (UAS)," in *Proc. IEEE Radar Conf. (RadarConf)*, May 2017, pp. 0669–0674.

[18] M. García-Fernández, Y. A. López, A. Arboleya, B. González-Valdés, Y. Rodríguez-Vaquero, M. E. D. C. Gómez, and F. L.-H. Andrés, "Antenna diagnostics and characterization using unmanned aerial vehicles," *IEEE Access*, vol. 5, pp. 23563–23575, 2017.

[19] G. Pupillo, G. Naldi, G. E. Bianchi, A. Mattana, J. A. Monari, F. E. Perini, M. A. Poloni, M. A. Schiaffino, P. Bolli, A. Lingua, and I. Aicardi, "Medicina array demonstrator: Calibration and radiation pattern characterization using a UAV-mounted radio-frequency source," *Exp. Astron.*, vol. 39, no. 2, pp. 405–421, Jun. 2015.

[20] J. L. Salazar, A. Umeyama, S. Duthoit, and C. Fulton, "UAS-based antenna pattern measurements and radar characterization," in *Proc. IEEE Conf. Antenna Meas. Appl. (CAMA)*, Sep. 2018, pp. 1–4.

[21] P. Bolli, G. Pupillo, F. Paonessa, G. Virone, S. J. Wijnholds, and A. M. Lingua, "Near-field experimental verification of the EM models for the LOFAR radio telescope," *IEEE Antennas Wireless Propag. Lett.*, vol. 17, no. 4, pp. 613–616, Apr. 2018.

[22] E. de Lera Acedo, P. Bolli, F. Paonessa, G. Virone, E. Colin-Beltran, N. Razavi-Ghods, I. Aicardi, A. Lingua, P. Maschio, J. Monari, G. Naldi, M. Piras, and G. Pupillo, "SKA aperture array verification system: Electromagnetic modeling and beam pattern measurements using a micro UAV," *Exp. Astron.*, vol. 45, no. 1, pp. 1–20, Mar. 2018.

[23] M. G. Fernandez, Y. A. Lopez, and F. L.-H. Andres, "On the use of unmanned aerial vehicles for antenna and coverage diagnostics in mobile networks," *IEEE Commun. Mag.*, vol. 56, no. 7, pp. 72–78, Jul. 2018.

[24] A. Y. Umeyama, J. L. Salazar-Cerreno, B. M. Wolf, and C. J. Fulton, "Recent development in UAV-based antenna pattern characterization for weather radars," in *Proc. IEEE Conf. Antenna Meas. Appl. (CAMA)*, Oct. 2019, pp. 199–202.

[25] M. Garcia-Fernandez, Y. A. Lopez, and F. L.-H. Andres, "Unmanned aerial system for antenna measurement and diagnosis: Evaluation and testing," *IET Microw., Antennas Propag.*, vol. 13, no. 13, pp. 2224–2231, Oct. 2019.

[26] M. G. Fernández, Y. Á. López, and F. Las-Heras, "Dual-probe near-field phaseless antenna measurement system on board a UAV," *Sensors*, vol. 19, no. 21, p. 4663, Oct. 2019.

[27] C. A. Balanis, *Antenna Theory: Analysis and Design*. Hoboken, NJ, USA: Wiley-Interscience, 2005.

ARTURO Y. UMEYAMA (Member, IEEE) received the B.S. degree in mechatronics engineering from the National University of Asunción, Asunción, Paraguay, in 2012, and the M.S. degree in electrical and computer engineering from The University of Oklahoma, Norman, OK, USA, in 2016, where he is currently pursuing the Ph.D. degree in electrical and computer engineering.

He is also a Graduate Research Assistant with the Advanced Radar Research Center, The University of Oklahoma. His research interests include advanced signal processing for weather radars, spectral analysis, and numerical radar simulation.

JORGE L. SALAZAR-CERRENO (Senior Member, IEEE) received the B.S. degree in ECE from University Antenor Orrego, Trujillo, Peru, the M.S. degree in ECE from the University of Puerto Rico, Mayagüez (UPRM), and the Ph.D. degree in ECE from the University of Massachusetts, Amherst, in 2011. At NCAR, he worked with the Earth Observing Laboratory (EOL) Division developing airborne technology for two-dimensional, electronically scanned, dual-pol phased array radars for atmospheric research. He joined the Advanced Radar Research Center (ARRC), The University of Oklahoma, as a Research Scientist, in July 2014. He was an Assistant Professor with the School of Electrical and Computer Engineering, in August 2015. His research interests include high-performance, broadband antennas for dual-polarized phased array radar applications, array antenna architecture for reconfigurable radar systems, APAA, Tx/Rx modules, radome EM modeling, millimeter-wave antennas, and development of low-cost dual-polarized active phased array antennas (APAA). He is a Senior Member of the IEEE Antennas and Propagation Society (AP-S). He received the Prestigious National Center for Atmospheric Research (NCAR) Advanced Study Program (ASP) Postdoctoral Fellowship and the Prestigious William H. Barkow Presidential Professorship from The University of Oklahoma for meeting the highest standards of excellence in scholarship and teaching, in 2019.

CALEB FULTON (Senior Member, IEEE) received the B.S. and Ph.D. degrees in electrical and computer engineering from Purdue University, West Lafayette, IN, USA, in 2006 and 2011, respectively. He is currently an Assistant Professor of electrical and computer engineering with the Advanced Radar Research Center, The University of Oklahoma, Norman, OK, USA. He is also involved in a number of digital phased-array research and development efforts for a variety of applications. His current research interests include antenna design, digital phased-array calibration and compensation for transceiver errors, calibration for high-quality polarimetric radar measurements, integration of low-complexity transceivers and high-power GaN devices, and advanced digital beamforming design considerations. He received the Purdue University Eaton Alumni Award for design excellence for his work on the Army Digital Array Radar Project, in 2009, the Meritorious Paper Award for a summary of these efforts from the 2010 Government Microcircuit Applications and Critical Technologies Conference, and the 2015 DARPA Young Faculty Award for his ongoing digital phased-array research.

• • •